KSCE Journal of Civil Engineering (2020) 24(3):962-974
DOI 10.1007/s12205-020-0072-8

pISSN 1226-7988, eISSN 1976-3808
www.springer.com/12205

Tunnel Engineering

Experimental Investigation of the Deformation and Failure Behavior of a Tunnel Excavated in Mixed Strata Using Transparent Soft Rock

Yuanhai Li[a,b], **Shuo Yang**[a], **Xiaojie Tang**[c], **Yanfeng Ding**[a], **and Qi Zhang**[d]

[a]*State Key Laboratory for Geomechanics and Deep Understrata Engineering, China University of Mining and Technology, Xuzhou 221116, China*
[b]*School of Mechanics and Civil Engineering, China University of Mining and Technology, Xuzhou 221116, China*
[c]*Dept. of Civil Engineering, The Univerisity of Hong Kong, Hong Kong 999077, China*
[d]*School of Civil Engineering, Southeast University, Nanjing 210096, China*

ARTICLE HISTORY

Received 15 January 2019
Revised 28 September 2019
Accepted 27 December 2019
Published Online 7 February 2020

KEYWORDS

Mixed strata
Transparent soft rock
Numerical simulation
Failure behavior
Failure process

ABSTRACT

To investigate the deformation and failure behavior of a tunnel excavated in mixed strata, transparent soft rock test and numerical simulations were performed. The distribution features of displacement and failure and the evolution laws were analyzed. In this study, a transparent material for simulating mixed strata was developed. The visualization of the spatial deformation inside rock masses will improve the understanding of this process. The tests suggest that the mechanical properties of transparent soft rock are similar to those of natural rock. Experiments on the isotropic and mixed strata conditions were carried out to study the deformation rules during tunnel boring machine (TBM) excavation. The test results show that the dominant deformation position and direction exist in isotropic and mixed strata. A shear slip band occurs in both mixed and isotropic strata but with different distributions. Finally, numerical simulations were conducted to study the failure process, and the damage pattern of the transparent soft rock experiment was similar to that of the numerical simulation. The interface of the softness and hardness layers controls the extension of rock damage.

1. Introduction

The recent development of tunnel boring machine (TBM) tunnels have led to tunnel faces consisting of mixed strata (Ramoni and Anagnostou, 2011; Zhang and Zhou, 2017). Mixed strata is characterized by the simultaneous presence of two or more geological materials on the tunnel face that exhibit significantly different material properties (Tóth et al., 2013). The mechanical properties of mixed strata normally appears to be approximately the same when the strata is parallel to the bedding direction. Moreover, a great difference is normally observed in the vertical direction. Tunnels constructed in complex rock strata may face many challenges and pose a great threat to the security of TBM engineering, with issues such as TBM jamming and shield damage (Mezger et al., 2017). Thus, understanding the deformation and failure behavior of a tunnel constructed in mixed strata is necessary for TBM excavation.

Physical model tests in a laboratory serve as an effective method for studying deformation and failure behavior and have the advantages of direct observation, the strict-control of the experimental conditions, the elimination of secondary factors and repeatability. Yong et al. (2006) studied the failure behavior, including the failure process and failure modes, of layered rocks influenced by the surrounding stress and layer angle Khanlari et al. (2015) analyzed the evolution rules of a sandstone fracture surface with different dip angles through the Brazil split test and uniaxial tests. A simulation model of horizontal mixed strata was built by Gong et al. (2015), and the process of tunnel instability was analyzed through thermal imaging technology. Most studies have mainly focused on multiple layered strata, and there is a lack of studies on excavation within mixed ground composed of an upper soft rock and a lower hard rock.

The traditional physical model methods are inevitably influenced by boundary conditions. In addition, because of the opaqueness of tests, internal deformation and failure behavior cannot be analyzed. For instance, the fracture zone cannot be detected in model experiment (Yang et al., 2018a), but it can be found through numerical simulation methods. Rock fracture normally happens

CORRESPONDENCE Shuo Yang yshappiness@163.com State Key Laboratory for Geomechanics and Deep Understrata Engineering, China University of Mining and Technology, Xuzhou 221116, China

inside the rock, and the fracture evolution rules of mixed strata cannot be fully obtained through opaque materials. Thus, a transparent rock method was put forward to study the internal failure behavior. However, transparent hard and isotropic rocks have been widely investigated, while the transparent materials for simulating mixed strata have rarely been investigated. For example, a uniaxial test was conducted on a flat glass pane with a signal crack to study the macroscopic failure path of crack growth (Brace and Bombolakis, 1963). Three-dimensional extension characteristics of cracks were studied through uniaxial and biaxial compression tests on cooling resin specimens with cracks (Dyskin et al., 1995). The stress distribution characteristics inside natural transparent coal rocks were studied through uniaxial compression tests based on three-dimensional stress freezing and photoelastic technology (Ju et al., 2014). The growth and distribution characteristics of cracks under the water face, and the influence on the occurrence and extension of 3D cracks by nonuniformities and surrounding pressures, were studied using 3D printing technology (Liu et al., 2016). Zhou et al. (2014; 2018b; 2019) and Yang et al. (2018b) studied the fracturing behavior of 3D flaws under uniaxial compression in Polymethylmethacrylate (PMMA) specimens.

An effective observation method is required for monitoring and recording the evolution of deformation and stress during physical experiments. Sensors are susceptible to the outside environment, meanwhile few measurement points are available. Computed tomography (CT) technology is applied to study the internal fracture of masses, but with limited data (Zhou et al., 2008; Teng et al., 2018). Digital image correlation method (DSCM) is characterized by its noncontact, multiple measurement-points and continuous observations (Zhou et al., 2018a; Li et al., 2019). The superiority of those methods makes it suitable for the analysis of the fracture evolution of surrounding rock.

Numerical simulation is also an effective method for studying the mechanical behavior of tunnels excavated in mixed strata (Aksoy et al., 2012; Hasanpour et al., 2014; Yang et al., 2017; Liu et al., 2018; Huang et al., 2019; Liu et al., 2019). Numerical simulation research related to mixed strata has mostly focused on the fracture pattern rather than the internal rock damage. Thus, the fracture evolution process of mixed strata has not be entirely understood. Moreover, general particle dynamics (GPD) (Zhou et al., 2015; Bi et al., 2016), peridynamics (PD) (Wang et al., 2016) and the extended finite element method (Zhou and Yang, 2012) have been used to study the fracture evolution process, but a limited number of studies have been carried out on mixed strata.

Although extensive research into the failure behavior of rock surrounding tunnels has been done, few model tests have been carried out to study the internal deformation and failure behavior of the upper-soft and lower-hard strata. In this study, the main aim is to investigate the internal deformation and failure behavior of tunnels in mixed strata. First, a transparent material for simulating mixed strata was developed. Then, physical model tests under isotropic and mixed strata conditions were conducted. The deformation rules and failure behavior of the rock surrounding tunnels were analyzed and compared. Finally, numerical simulations were conducted to study the failure process. The results of the physical model tests and numerical simulations were analyzed and compared.

2. Physical Experiment and Numerical Simulation Design

2.1 Development of Transparent Soft Rock to Simulate Mixed Strata

To make transparent soft rock, silicon powder and mineral oil were chosen as an aggregate and a cementitious agent respectively, because of their good transparency and stability as well as their

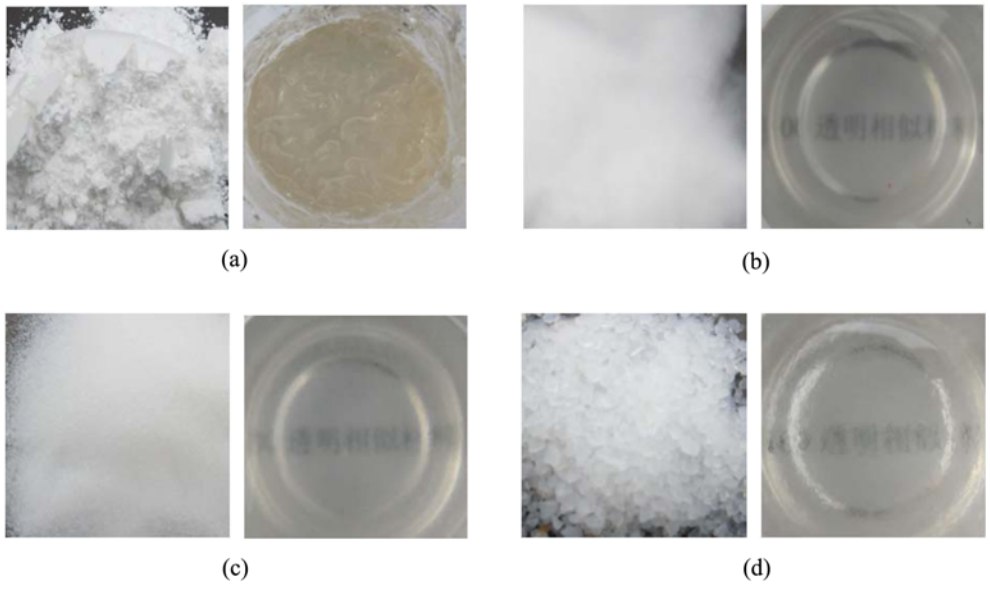

Fig. 1. Transparent Soft Rock Prepared by Different Silicon Powder Sizes: (a) 10 μm, (b) 48 μm, (c) 550 μm, (d) 1,700 μm

similar refractive index values. A series of trial tests were performed to select the best particle size of silicon powder to enable the samples to provide the best transparency. As shown in Fig. 1, silicon powder with a particle size of 48 μm exhibits the best transparency. The mass ratio of silicon powder and mineral oil is 0.6. As shown in Fig. 2, the strength of the transparent soft rock is mainly determined by consolidation stress and time. The strength of the sample consolidated for 15 days are obvious larger than the strengths of the others samples. There should be a positive correlation between the consolidation stress and the strength. Thus, the relatively long consolidation time and the high consolidation stress lead to the high strength. Fig. 3 shows the test results of the elastic modulus, the cohesion and the friction of the transparent soft rock samples. If the consolidation stress is too large, then the model easily exhibits low transparency after consolidation and unloading; Thus, a consolidation stress of 1.0 MPa was used for the transparent soft rock test model.

To simulate mixed strata, two transparent soft rock ratios were tested. The hardness-downward layer 1 is made of a 48-μm silica powder. The softness-upward layer 2 is made by mixing 48-μm and 550-μm silica powders at a volume proportion of 10:1, which we determined through contrast tests to meet the strength simulation. By increasing the volume proportion of 550-μm silica powder, the layer 2 was simulated for softness-upward strata. The basic mechanical parameters are shown in Table 1. Transparent soft rock should be consolidated for 30 days, and the consolidation stress was 1.0 MPa. The transparent soft rock samples with different strength property values were used to simulate the softness-upward and hardness-downward mixed strata.

In the transparent soft rock test for the simulation of TBM tunneling, the characteristics of the fracture surrounding the rock are similar to those of the traditional material comprised of river

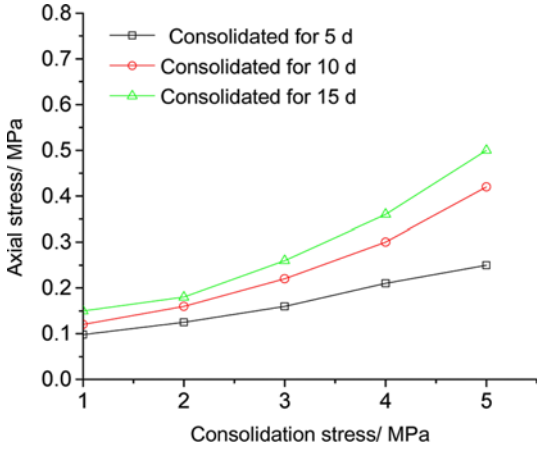

Fig. 2. Test Results of the Uniaxial Compressive Strength of the Transparent Soft Rock Samples

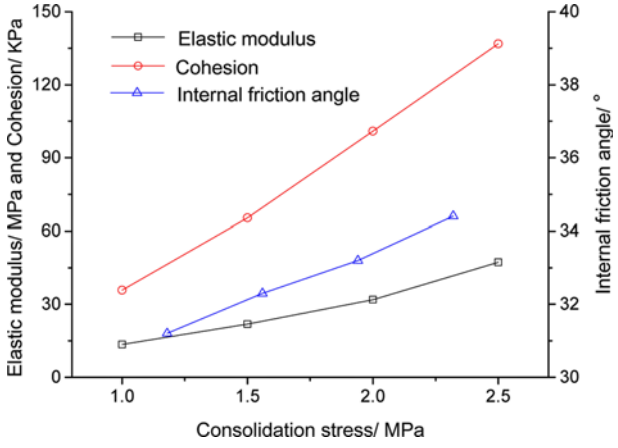

Fig. 3. Test Results of the Elastic Modulus, the Cohesion and the Friction of the Transparent Soft Rock Samples

Table 1. Basic Mechanical Parameters of the Similar Transparent Material

Lithology	Uniaxial compressive strength (MPa)	Lateral pressure coefficient (K_0)	Cohesion (MPa)	Internal friction angle (°)	Elastic modulus (MPa)	Poisson's ratio
Layer 1	0.21	0.31	0.095	33.1	30.00	0.29
Layer 2	0.13	0.28	0.058	25.2	19.10	0.31

Fig. 4. The Similar Characteristics of the Transparent Soft Rock Compared to an Ordinary Material and Natural Rock (Li and Lin, 2015): (a) Transparent Soft Rock, (b) A Similar Ordinary Material, (c) Triaxial Stress-Strain Curve

sand and paraffin, as illustrated in Figs. 4(a) and 4(b). After the test, the transparent rock model was cut from centre to clearly reveal the similar fracture characteristics, such as the zonal disintegration phenomenon. This phenomenon of the transparent soft rock is an important difference from transparent soil, and transparent soft rock technology has also proven to be an effective material for simulating a rock mass.

The mechanical properties of the transparent soft rock are similar to those of natural rock (Li and Lin, 2015). As shown in Fig. 4(c), the confining pressures are 0.3 MPa, 0.45 MPa, 3 MPa and 1.5 MPa, the particle size of the silicon powder in the transparent soft rock is 48 μm, and the loading rate is 0.1 mm/min. The mechanical properties of the transparent soft rock are similar to expansive mudstone according to the conventional three axis test. In addition, as shown in Fig. 12, after the peak value, there is obvious strain softening, in agreement with the deformation and failure characteristics of the surrounding rock in soft rock and the deep high stress environment.

2.2 Physical Experimental Design

2.2.1 Sample Preparation

The formation of mixed strata is complex, with the double-layer structure characterized by a softness-upward layer and a hardness-downward layer being the most typical. As shown in Fig. 5, specimens with two types of transparent soft rock strengths are made for mixed strata, and one type is made for isotropic strata.

As shown in Fig. 6, the transparent soft rock was made through configuration, vacuum-pumping, laying down a speckle surface and consolidation. Special attention should be paid to the following matters regarding the preparation. Constant sloshing of the vacuum box allows the bubbles in the transparent material to be more easily expelled. A transparent plastic film should be placed on the inner wall of the mold to protect the sample when removing the mold. During loading and unloading, the pressure process should be multilevel. All efforts were made to ensure the transparency of the samples, so that the internal deformation and fracture evolution rules could be obtained.

To measure the internal deformation, the laser test is widely

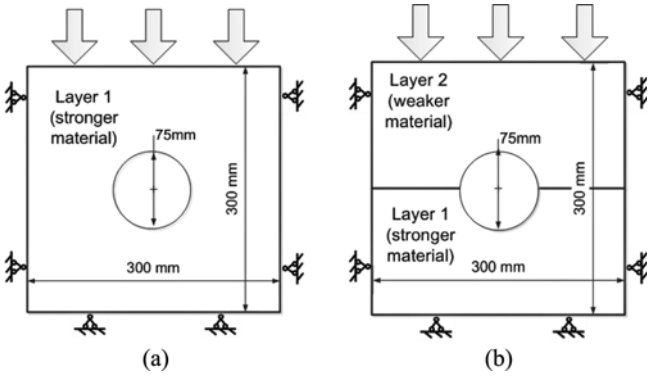

Fig. 5. Formation Combination of TBM Model: (a) Isotropic Strata, (b) Mixed Strata

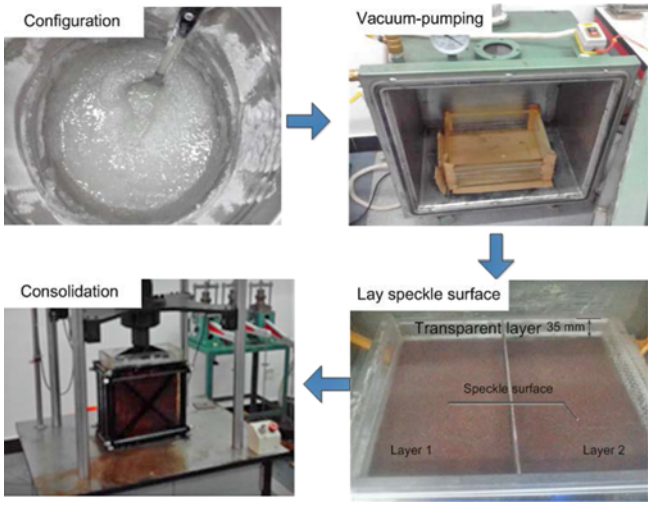

Fig. 6. Preparation of the Similar Transparent Materials for Mixed Strata

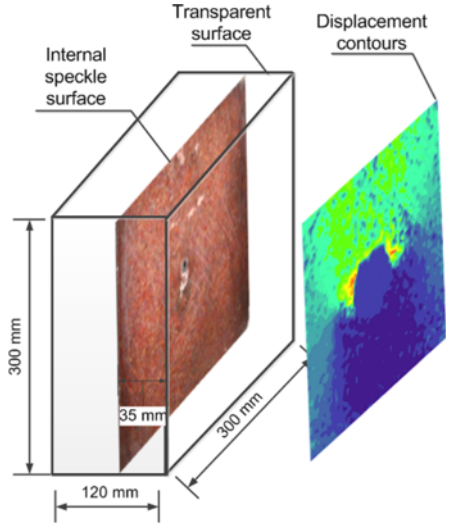

Fig. 7. Internal Observation of the Tunnel Model Section

used in transparent soil tests (Iskander et al., 2015; Sun and Liu, 2014). The principle of the laser test is based on particle image velocimetry (Ahmed and Iskander, 2012), which is not appropriate for use in transparent soft rock because transparent soft rock with an isotropic and dense structure is completely different from transparent soil (Fig. 4). Thus, artificial internal speckles were in the internal model for the DSCM measurement (Lee and Yoo, 2006). As shown in Fig. 7, the internal speckle surface was placed 35 mm inside the surface. The internal speckle surface was made from a dyed silica powder, which provides rich textural features for the global deformation measurements.

2.2.2 Test Setup and Procedure

As shown in Fig. 8, a plane-strain model experimental system was designed, consisting mainly of three parts: a loading system, a digital camera system, and a tunneling device.

The sample molds were made of a steel frame and Perspex, with inner dimensions of 300 mm × 120 mm × 300 mm (length

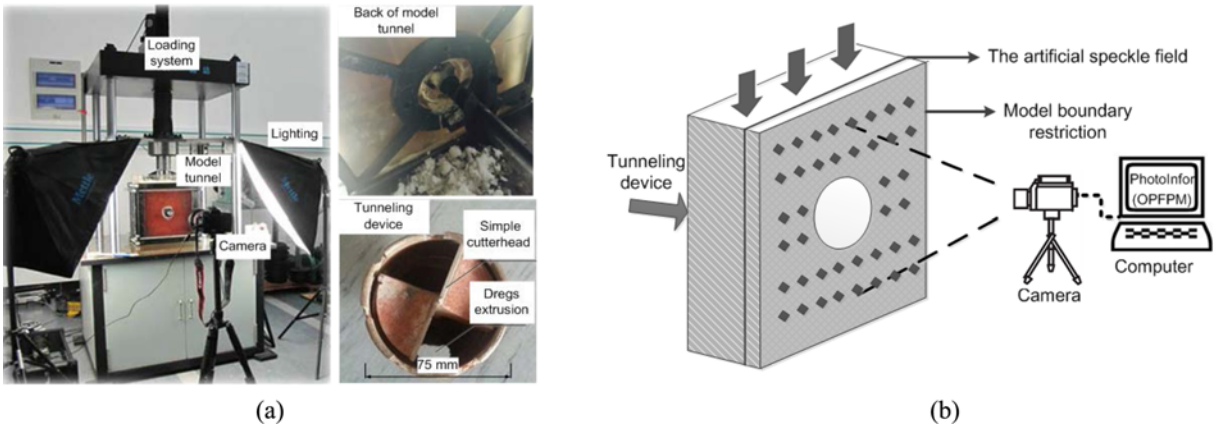

Fig. 8. Test Setup: (a) Pictures of Test Setup, (b) Schematic Layout of Test

× width × height), which enable the strict boundary restriction during the test. Despite the uniaxial loading, the transparent similar material was under a Poisson force in the horizontal direction, with the constraint of the model box all around. A tunneling device was specially designed to simulate tunnel excavation. The device was made of a specially designed drill bit, with an inner diameter of 75 mm.

A Canon 6D digital camera with a resolution of 5472 × 3648 pixels was used to capture the images. Then, the rock-surface images were analyzed by the self-developed DSCM analysis software-PhotoInfor. The accuracies of the measurements by PhotoInfor have been suggested based on both theoretical analysis and experimental tests (Li et al., 2019). The one point and five pixel blocks method (OPFPM) algorithm of PhotoInfor was used to analyze the deformation surrounding the tunnel while cracks appear.

Transparent soft rock is similar to natural rock; according to similar calculations, the strength of transparent soft rock is equal to 21.53 MPa in practice. The strengths of layer 1 and layer 2 are 21.53 MPa and 10.99 MPa, respectively. The bulk density of a similar transparent material is approximately 10.7 kN/m^3. The geometry similarity C_L and the bulk density similarity C_γ are 40 and 2.29, respectively. Thus, the size of the simulated actual rock mass is 12 m × 4.8 m × 12 m.

The simulation indexes of concern are enumerated in Eq. (1) (Li et al., 2019). The quantitative relationships between the similarity ratios can be calculated based on a dimensional analysis, and therefore, the equations related to the indexes are revealed in Eq. (2). The geometric similarity ratio is set as 40 (C_L = 40), and the gravitational acceleration ratio is set as 1 (C_g = 1). Consequently, the time similarity ratio can be calculated (C_t = 6.32) based on Eq. (2).

$$f(L,\sigma,\varepsilon,\upsilon,\sigma_t,\sigma_c,\delta,E,\gamma,g,t,\varphi,C)=0 \tag{1}$$

$$\begin{cases} C_\delta C_\gamma = C_C \\ C_g C_t^2 = C_\delta = C_L \\ C_C = C_\sigma = C_{\sigma t} = C_{\sigma c} = C_E \\ C_\varepsilon = C_\mu = C_\varphi = 1 \end{cases} \tag{2}$$

where C_σ, C_E, C_C, C_ε, C_φ and C_μ are the similarity ratios of stress, elastic modulus, cohesion, strain, friction angle, and Poisson's ratio, respectively.

To measure the internal deformation, an appropriate measurement method is also required. The digital photogrammetry method is widely used in geotechnical model experiments as a general measurement technology. The algorithm for processing the digital photographs is based on the DSCM, which recognizes the speckles by calculating the correlation coefficient of the gray values of the pixel blocks.

The fracture reduces the correlation coefficient, leading to errors. For example, Li et al. (2014) studied the failure mode of soft rock though DSCM but ignored the effects of fracture. As shown in Fig. 4(a), shear and slip failure will inevitably result in the failure of conventional measurement methods. OPFPM (Li et al., 2016) was used to measure the large deformation while cracks appear. This method avoids the low image correlation caused by cracks. Therefore, the misjudgement of image pixels is reduced, and the large deformation analysis accuracy is improved. The OPFPM algorithm finds a pixel block not crossing the crack that can avoid low image correlation caused by the fracture.

The transparent soft rock model should be consolidated for 30 days until reaching the target strength. Under multistage loading, the model load reached 0.2 MPa as the initial strata vertical stress after consolidation. The details of the steps involved are as follows:

Step 1: The computer, loading system, digital camera, and software functioned normally after all the instruments were arranged. The digital camera was set 0.5 m in front of the observation surface and the parameters were adjusted to obtain distinct images. Next, two photography luminaires were set towards the observation surface along with the shading cloth used to block out the outside light to ensure that the level of lighting remained stable during the test process.

Step 2: The time similarity ratio and the geometric similarity ratio are 6.32 and 40, respectively, as determined by theoretical calculations. According to relevant information, the TBM tunnel

Table 2. Basic Mechanical Parameters of the Simulation Model

Lithology	Cohesion (MPa)	Internal friction angle (°)	Elastic modulus (MPa)	Poisson's ratio	Tensile strength (MPa)	Dilation (°)	Plastic strain ratio	Yield ratio	Elastic Reduction Ratio
Layer 1	0.095	33.1	30.00	0.29	0.010	4.2	0.032	0.8	0.5
Layer 2	0.058	25.2	19.10	0.31	0.004	3.1	0.040	0.8	0.5

in a practical situation is excavated at 10 to 100 meters per day, and the working time is 12 hours each day, which is divided into two working parts: Excavation for 6 hours and equipment maintenance for 6 hours. In this test, a practical TBM tunnel was assumed to be excavated at the rate of 10 meters per day and the model excavation rate was 1.7 meters per hour based on the calculations. The excavation time was calculated to be 27 mins. The tunnel was excavated at one time.

Step 3: After the tunnel excavation, the initial strata stress was kept steady for 20 mins during the observation of the deformation and the stress change. Next, we continued to perform step loading in increments of 0.1 MPa along the vertical direction for one step. Each step was held for 20 mins, and the rock deformation as well as the stress variation were observed and monitored until tunnel collapse. Every 2 seconds, the images were collected during all the steps.

2.3 Numerical Model Construction

To verify the results of the physical experiments and further explore the evolution rules of rock failure in mixed strata, numerical simulations were also carried out by using FLAC^{3D}. The basic mechanical parameters used for the simulation are listed in Tables 1 and 2, and were obtained by the calculations and simulated uniaxial compressive tests. As shown in Fig. 9, a damage-softening constitutive model (Yang et al., 2019) was used to simulate the internal rock damage.

The simulated stress–strain curves for layer 1 and layer 2 are shown in Fig. 10(a). The samples were characterized by their ductile failure for comparatively greater soft deformations in the post-peak deformation stage. The peak value of the numerical simulation cannot coincide with the experiment that the strain value of the numerical simulation will be comparatively smaller, which normally caused by the impossibility of simulating the situation of rock compaction through numerical methods.

A two-dimensional simulation model (Fig. 10(b)) with the

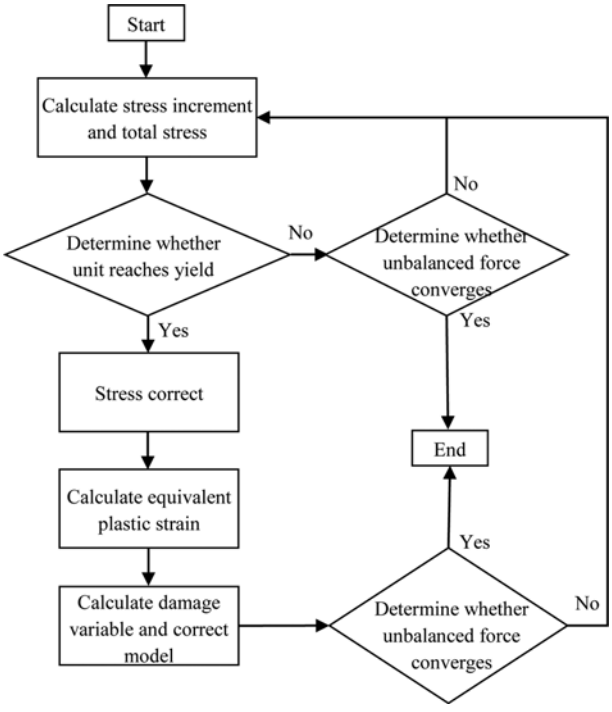

Fig. 9. Damage-Softening Constitutive Model in FLAC^{3D} (Yang et al., 2019)

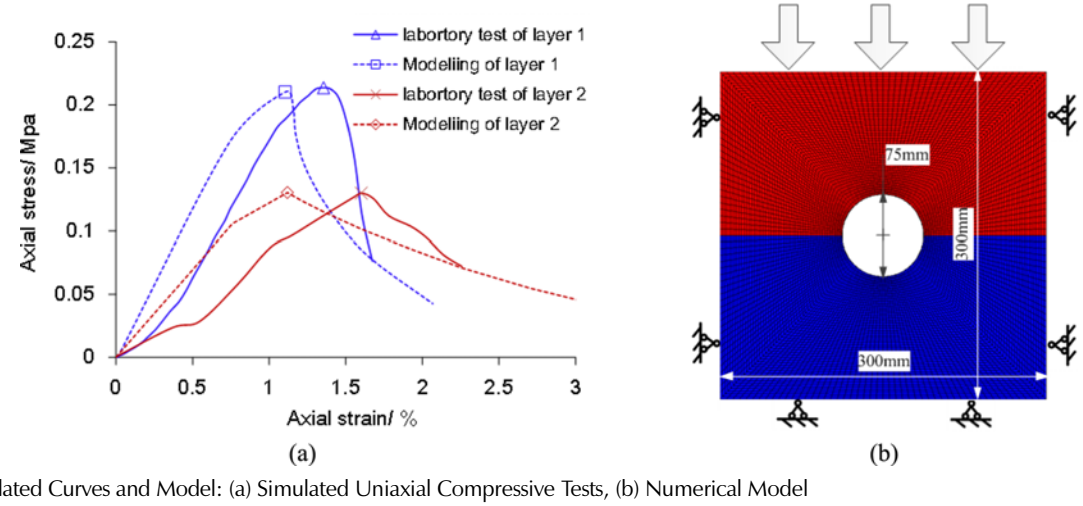

Fig. 10. Simulated Curves and Model: (a) Simulated Uniaxial Compressive Tests, (b) Numerical Model

same dimensions as the physical model was created, containing 10000 blocks. The boundary conditions and loading method for the numerical model are the same as those for the physical model.

3. Evolution of Rock Deformation and Fracture Surrounding a Tunnel

3.1 Analysis of the Surrounding Rock Deformation

The field of surrounding rock displacement obtained through Photoinfor is shown in Fig. 11. The analysis grid contained 3721 blocks with 50 pixels between two measuring points. It was found that the dominant deformation position and direction exist in isotropic and mixed strata. As can be revealed from Fig. 11(a), the instability of isotropic strata is a gradual process of tunnel failure. After the excavation, rock deformation first occurs at the tunnel roof (graph A1) and then transfers to the sidewalls along with the roof failure (graph A2), intensifying the shear failure of the sidewall. Finally, the tunnel collapses after the breakdown of both the tunnel roof and the sidewalls (graph A3). Displacement occurs mostly at the sidewalls, with no evident floor bulge phenomenon. The instability process of softness-upward and hardness-downward mixed strata is revealed in Fig. 11(b); evident displacement first occurs at the sidewalls and the tunnel floor (graph B1). The range of the plastic area extends during the tunnel failure (graph B2), and the roof collapse and the floor bulge occur last. The deformation of the mixed strata primarily occurs at the sidewalls and the roof, accompanied by the evident floor bulge phenomenon, with its maximum deformation occurring at an angle of 45 degrees from the horizontal plane (graph B3).

Deformation at the roof, floor and sidewalls of the tunnel formed as a whole system (graph B3), with the shrinking of the

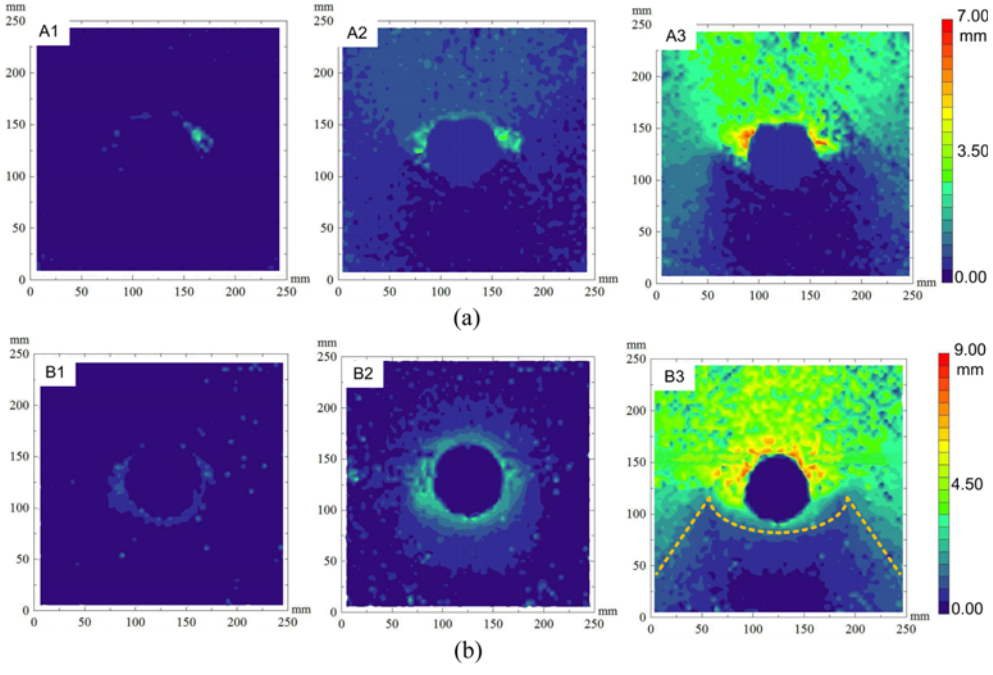

Fig. 11. Internal Displacement Charts of the Surrounding Rocks: (a) $\sigma_{vertical}$ of Isotropic Strata (A1: 0.2 MPa, A2: 0.4 MPa, A3: 0.6 MPa), (b) $\sigma_{vertical}$ of Mixed Strata (B1: 0.2 MPa, B2: 0.4 MPa, B3: 0.6 MPa)

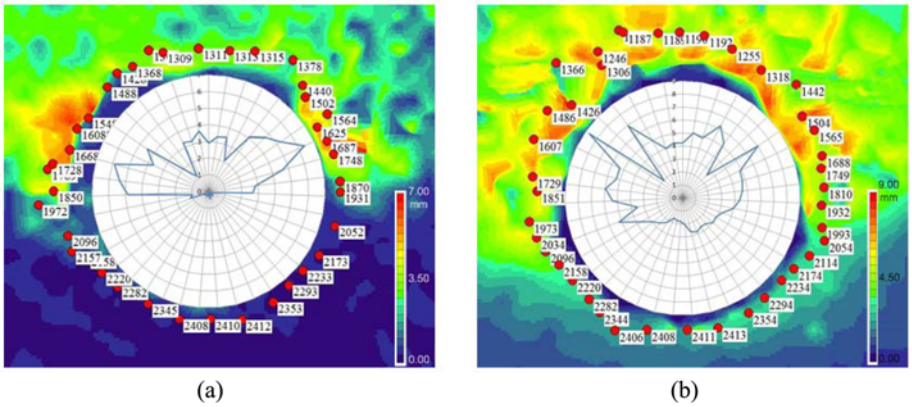

Fig. 12. Internal Displacement of the Rocks around the Tunnel: (a) Isotropic Strata, (b) Mixed Strata

sidewalls and the roof collapse contributing to the floor bulge. Deformation at the isotropic strata primarily occurs at the sidewalls to achieve a comparatively better sustainability of the tunnel roof; therefore, no bulge occurs at the floor (graph A3).

The dominant deformation position and direction in the isotropic and mixed strata conditions are also found, as indicated by the comparison between Figs. 12(a) and 12(b).

Displacement-time curves were drawn based on the position data of the tunnel roof, the tunnel floor and the sidewalls to study the displacement evolution of the surrounding rocks. As can be revealed in Fig. 13, a global slippage tendency of the surrounding rocks occurs with the deformation difference of each of the measurement points.

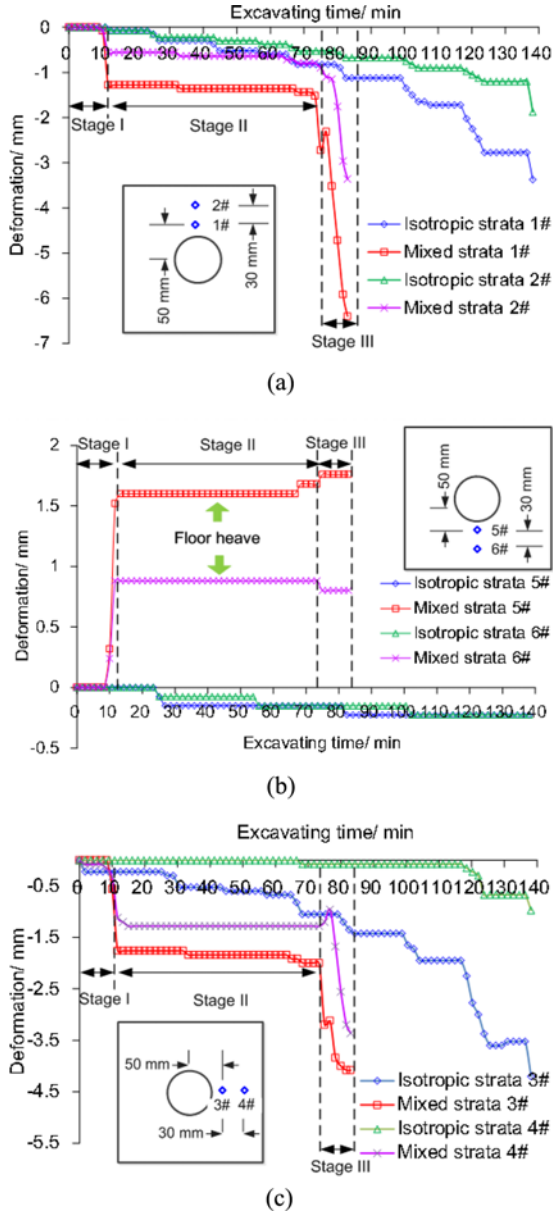

Fig. 13. Comparison of the Radial Displacement in the Surrounding Rock: (a) Vertical Deformation in Roof, (b) VerticaL Deformation Curves in Floor, (c) Horizontal Deformation in the Right Wall

A more evident phase characteristic occurs in mixed strata than in isotropic strata. As shown in Figs. 13(a) and 13(b), three deformation stages of the mixed strata were analyzed. The deformation rate becomes faster after 9 min of excavation, and then the tunnel deformation reaches a stable state. After 75 min, tunnel collapse occurs with a continuous increase in the deformation rate. Elastic rock deformation at early excavation is revealed in Stage I, when the surrounding stress is less than the elastic strength, and plastic deformation occurs when the surrounding stress exceeds the elastic strength. A stable transition of rock deformation after the stress adjustment is reflected in Stage II. Stage III reveals that the rock deformation will exceed the limit of the surrounding rocks, without a support structure, when the plastic zone extends to some extent. As shown in Fig. 13(b), an evident floor bulge occurs in the mixed strata but not in the isotropic strata. The deformation rate increases after 9 min of excavation, and then the tunnel deformation reaches a stable state. Rock deformation in layer 2 of the mixed strata exceeded the ultimate strength after 75 min of excavation, and a gradual deformation occurred in Stage III under the residual strength at the tunnel roof and the sidewalls.

The phase characteristic lies the fact of floor heave in mixed strata, as shown in Fig. 13(b). The deformation of mixed strata remains stable after the floor heave, and the presence of hard rock strata could reduce the deformation in soft rock (Yang et al., 2018a), which is further analyzed in Fig. 17.

3.2 Analysis of the Surrounding Rock Fractures

The distribution rules of the maximum shear strain are obtained through transparent soft rock technology, as shown in Fig. 14. The OPFPM algorithm provides a high accuracy for measurements when cracks appear.

A shear slip band occurs in both the mixed and isotropic strata but with different distributions, as accompanied by a conspicuous distinction of the maximum shear strain around the tunnel (Fig. 14(c)). The slip band in the isotropic strata occurs at the sidewalls. However, the distribution of the slip band in the mixed strata is distinct and is spread at an angle of 45 degrees from the horizontal plane.

The fracture evolution rules of the isotropic strata are revealed in Fig. 14(a). The cracks first occur at the right side of the tunnel during the excavation (graph A1). The crack does not simultaneously occur in the left wall because it is difficult to achieve an absolutely uniform material and uniform loading. Cracks occur at the sidewalls when loaded at 0.4 MPa (graph A2) and extend to the outside along with the occurrence at the roof under an increasing load (graph A3). The observed phenomenon can be explained by the high cyclic compressive stress concentration that arises around the tunnel walls under the vertical condition of maximum loading direction and tunnel axes. Moreover, compressed shear failure will consequentially occur at the sidewalls based on the Mohr - Coulomb strength theory (Li et al., 2014). The failure mode of the isotropic strata is shown in Fig. 18(a). Several cambered shear slip bands are generated at the sidewalls to

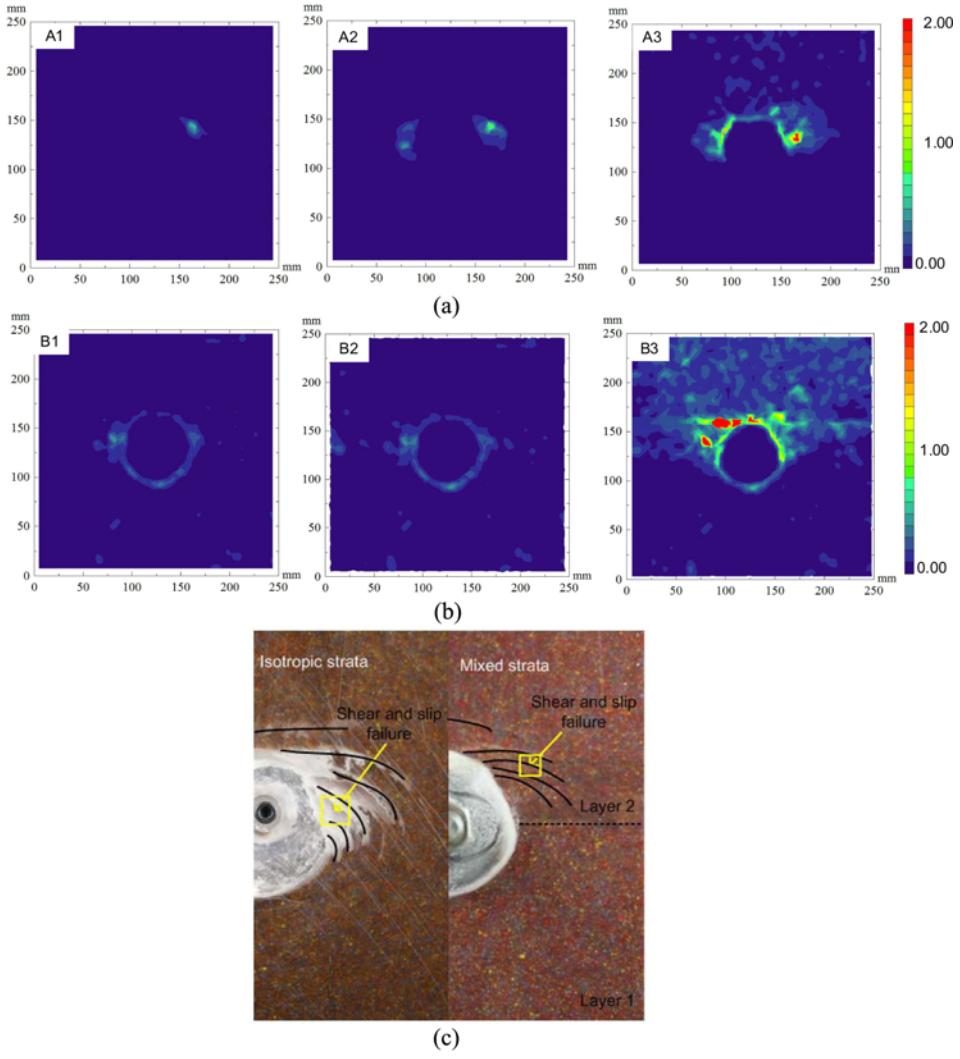

Fig. 14. Internal Maximum Shear Strain Charts of the Surrounding Rocks: (a) $\sigma_{vertical}$ of Isotropic Strata (A1: 0.2 MPa, A2: 0.4 MPa, A3: 0.6 MPa), (b) $\sigma_{vertical}$ of Mixed Strata (B1: 0.2 MPa, B2: 0.4 MPa, B3: 0.6 MPa), (c) Shear Slip Band in Isotropic Strata and Mixed

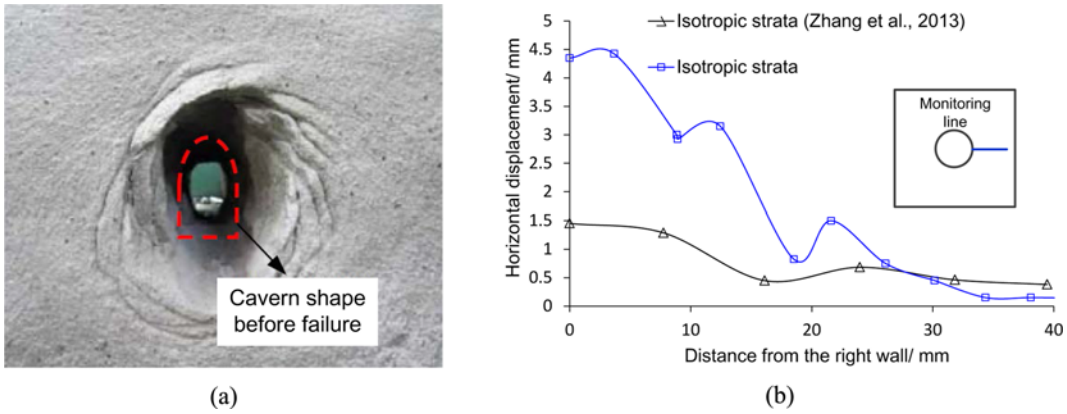

Fig. 15. Comparison of the Spiral-Shaped Damage Zone: (a) Similar Damage Zone (Zhang et al., 2013), (b) Comparison of the Relative Radial Displacement

reveal the compressed shear failure characteristics, thus verifying the analysis above.

The failure evolution of the mixed strata is revealed in Fig. 14(b); Cracking first occurs at the roof and sidewalls of the tunnel (graph B1) and then extends to the outside. There is no obvious change in the maximum shear strain during an increased load, as revealed in graph B1 and B2, in contrast to graph A1 and A2. Sliding linear failure occurs at the upper rock of the tunnel

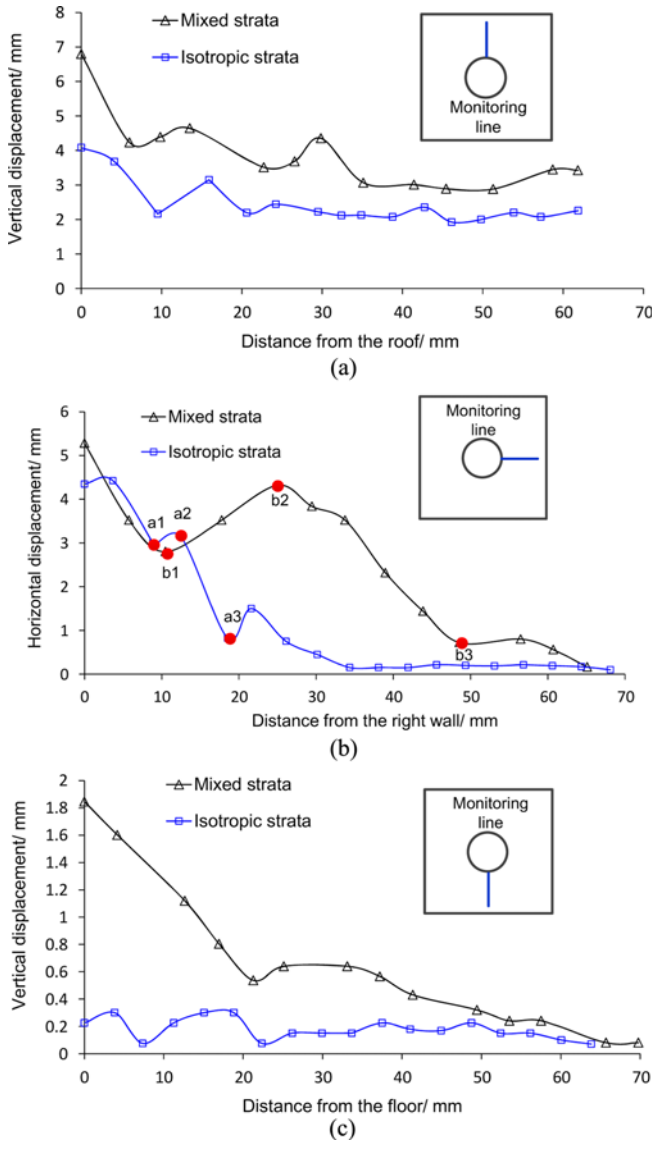

Fig. 16. Comparison of the Radial Displacement at Stage III: (a) Vertical Displacement in Roof, (b) Horizontal Displacement in the Right Wall, (c) Vertical Displacement in Floor

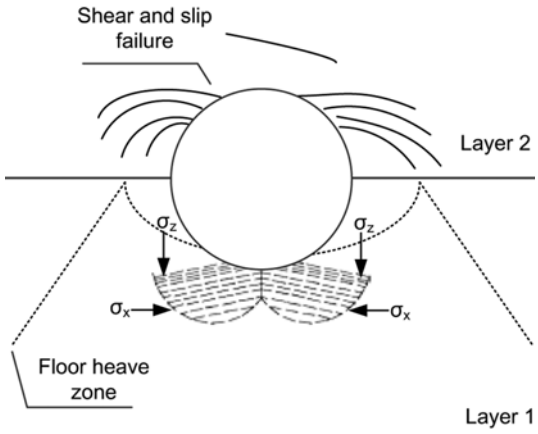

Fig. 17. Failure Behavior of a Tunnel Excavated in Mixed Strata

because of its comparatively lower rock strength. The ultimate strain first reached at the softness-upward layer and led to tunnel damage (graph B3).

In the case of spiral-shaped damage zone (Fig. 15(a)), sidewall rock fails by shear bands that are localized around the cavern and are spiraling outward from the sidewall, which shows similar fracture characteristics of isotropic strata (Fig. 14(c)). Moreover, the radial displacement also exhibits the same fluctuation features due to spiral-shaped damage zone.

Fluctuations in the radial displacement curves are shown in Fig. 16, with an interval distribution between the peak and the trough; this characteristic is different from that of the displacement around the excavated tunnel, and it decreases with a longer distance to the excavation surface in shallow buried tunnels (Li et al., 2014). The shear sliding band inside the transparent soft rock (Fig. 4) serves as a key factor for the curve fluctuation and is similar to the evolution in deep buried strata (Chen et al., 2013; Zhou and Shou, 2013; Zhang et al., 2017). As shown in Fig. 16(b), the failure zones are distributed at the trough positions (a1, a3, b1, b3), and the stable zones are distributed at the peak areas (a2, b2). The same phenomenon extends to the roof and the floor.

The surrounding rock fractures between the mixed and isotropic strata show different damage forms. As shown in Fig. 16(b), the curves show the same trend near the wall, while in Fig. 16(c), the curves show the completely different trend, because compressed shear failure in the wall occurs in both the isotropic and the mixed strata, while floor bulge occurs only in the mixed strata.

The floor heave zone and the shear and slip failure function as a whole system. As shown in Fig. 17, shear and slip failure happens at the roof and side walls in mixed ground due to its comparatively lower rock strength. Moreover, the surrounding rocks in these areas are not capable of bearing force, and σ_z is transmitted below. Finally, the tunnel bottom will lose the bearing force when rock failure happens around the bottom position. σ_x therefore happens at the bottom of the tunnel shrink, and the floor heave zone occurs at last with the compressed rock bending when the critical load is reached.

3.3 Analysis of the Surrounding Rock Failure Process

Numerical simulations were conducted to study the failure process under isotropic and mixed strata conditions. As shown in Fig. 18(a), significant stress concentration happens at each side of the circular tunnel within the isotropic strata during loading (graph A1). Shear damage occurred first on both sides of the surrounding rock when the concentrated stress exceeds the rock shear strength (graph A2). During the increment of vertical loading, the damage area of surrounding rock gradually extends from the left and right sides of the tunnel to the top and floor of the tunnel (graph A3). The damage pattern of the model shows the approximate symmetry for its symmetric model structure and exterior loading conditions.

In regard to Fig. 18(b), stress concentration happens at the horizontal direction of the circular tunnel during the loading

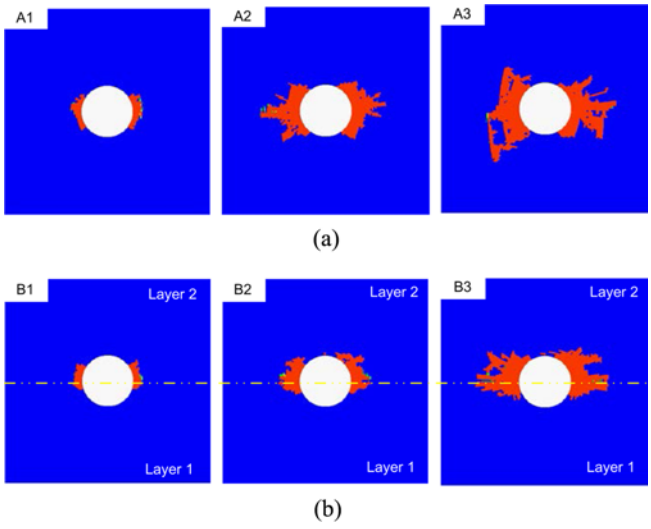

Fig. 18. Simulated Failure Process: (a) Isotropic Strata, (b) Mixed Strata

within the mixed strata (graph B1). Because of the lower strength of the softness-upward layer compared to the hard layers, failure damage happens first at both sides of the tunnel within the softness layer area (graph B2). Rock damage happened within the soft area contributes to the internal structural adjustment and stress redistribution of the model, and then the damage area extends to the top of the model. The model comes to a residual deformation stage when the damaged area of the surrounding rock extends to the model boundary (graph B3). It should be noted that the damage area of the softness layer can no longer expand when it extends to the hardness layer, which shows that the interface of the softness and hardness layers can control the extension of damage.

Figure 19 demonstrates that the damage pattern of the transparent soft rock experiment is similar to that of the numerical simulation. The internal maximum shear strain charts of the physical experiment and the numerical simulation follow the same distribution law. As shown in Fig. 19(a), through numerical simulations, damage areas occur on both sides of the tunnel, and there is a connection between the areas. In contrast, as seen from the transparent soft rock test image, shear slip failure occurred in the sidewalls of the tunnel. Moreover, cracks start to connect within the two damage zones. Fig. 19(b) shows that the damage zone occurs intensively in the area of 45 degrees, and connects to the damage zone above the tunnel. The rock damage pattern based on numerical simulations is similar to that of the experiment.

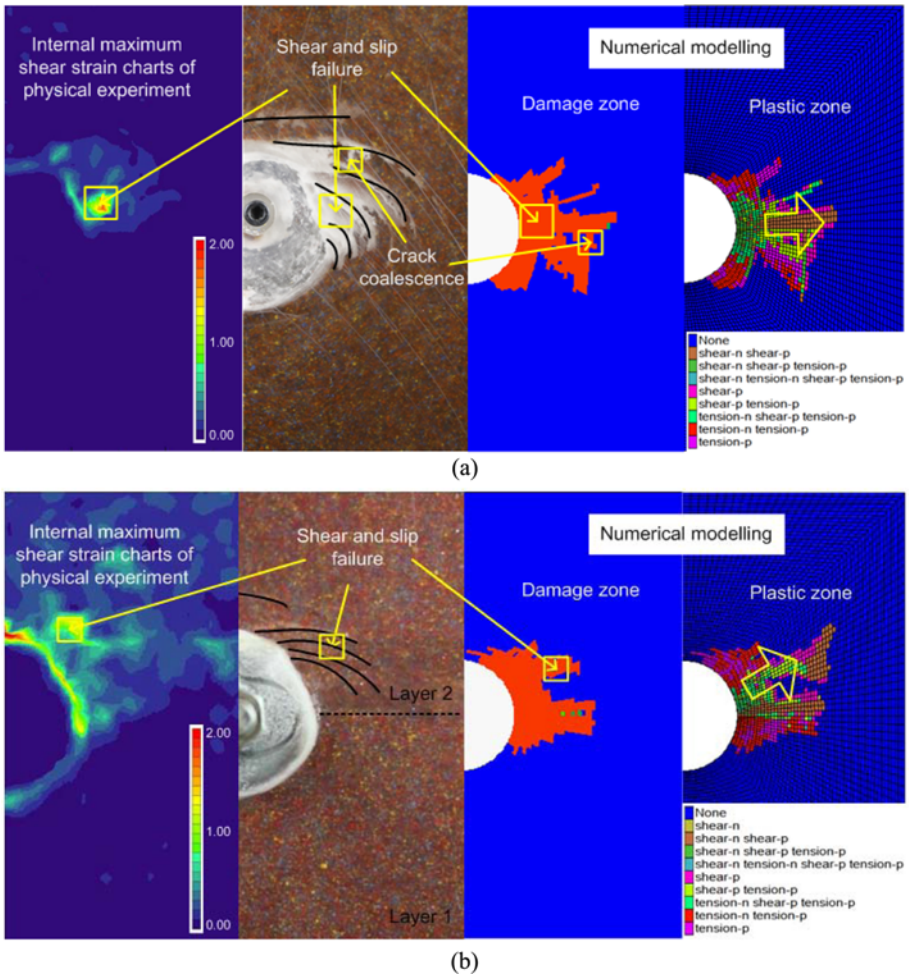

Fig. 19. Failure Mode of Physical Experiment and Numerical Modeling: (a) Isotropic Strata, (b) Mixed Strata

As seen from plastic zone (Fig. 19), a dominant failure position and damage direction exist in isotropic and mixed strata. Damage of the isotropic strata primarily occurs at horizontal plane, while that of mixed strata occurs at an angle of 45 degrees from the horizontal plane. Shear damage dominants the failure process with tensile damage spreads from its two wings.

4. Conclusions

In this study, both physical model tests and numerical simulations under isotropic and mixed strata conditions were conducted to study the internal deformation and failure behavior of tunnels in mixed strata. Based on the experiment results, the following conclusions can be drawn:

1. A new transparent material for simulating mixed strata was developed. The mechanical properties of transparent soft rock are similar to those of natural rock. The fracture characteristics of transparent soft rock, such as the zonal disintegration phenomenon, are importantly different from those of transparent soil.
2. A dominant deformation position and direction exist in isotropic and mixed strata. The surrounding rock fractures also show different damage forms. Internal displacement of the isotropic strata primarily occurs at the sidewalls, while deformation of the mixed strata primarily occurs at the sidewalls and the roof and is accompanied by the evident floor bulge phenomenon, with its maximum deformation occurring at an angle of 45 degrees from the horizontal plane. Fluctuations in the radial displacement curves shown a different trend, because compressed shear failure in the wall occurs in both isotropic and mixed strata, and floor bulge occurs only in the mixed strata.
3. The damage pattern of the transparent soft rock experiment is similar to that of the numerical simulation. The damage area occurs from the sidewalls to the exterior within the isotropic strata. In the mixed strata, the damage area occurs intensively in 45 degree area, connecting to the damage zone above the tunnel. Meanwhile, the interface of the softness and hardness layers controls the extension of the rock damage. The damage area of the softness layer can no longer expand when it extends to the hardness layer.

Acknowledgements

This research was supported by the National Basic Research Program of China (973 Program) Grant No. 2014CB046905 and the National Natural Science Foundation of China (No.51174197). Additionally, the authors are grateful to the anonymous reviewers of this article for their careful reading of our manuscript and their many helpful comments.

ORCID

Yuanhai Li https://orcid.org/0000-0003-4526-8775

Shuo Yang https://orcid.org/0000-0001-9166-407X

References

Ahmed M, Iskander M (2012) Evaluation of tunnel face stability by transparent soil models. *Tunnelling and Underground Space Technology* 27(1):101-110, DOI: 10.1016/j.tust.2011.08.001

Aksoy CO, Ogul K, Topal I, Ozer SC, Ozacar V, Posluk E (2012) Numerical modeling of non-deformable support in swelling and squeezing rock. *International Journal of Rock Mechanics and Mining Sciences* 52:61-70, DOI: 10.1016/j.ijrmms.2012.02.008

Bi J, Zhou XP, Qian QH (2016) The 3D numerical simulation for the propagation process of multiple pre-existing flaws in rock-like materials subjected to biaxial compressive loads. *Rock Mechanics and Rock Engineering* 49(5):1611-1627, DOI: 10.1007/s00603-015-0867-y

Brace WF, Bombolakis EG (1963) A note on brittle crack growth in compression. *Journal of Geophysical Research* 68(12):3709-3713, DOI: 10.1029/JZ068i012p03709

Chen XG, Zhang QY, Wang Y, Li SC, Wang HP (2013) In situ observation and model test on zonal disintegration in deep tunnels. *Journal of Testing and Evaluation* 41(6):1-11, DOI: 10.1520/JTE20120336

Dyskin AV, Germanovich LN, Jewell RJ, Joer H, Krasinski JS, Lee KK, Roegiers JC, Sahouryeh E (1995) Some experimental results on three-dimensional crack propagation in compression. *Bulletin of the American Mathematical Society* 31(240):1-10, DOI: 10.1090/S0002-9904-1925-03982-8

Gong W, Peng Y, Sun X, He M, Zhao S, Chen H, Xie T (2015) Enhancement of low-contrast thermograms for detecting the stressed tunnel in horizontally stratified rocks. *International Journal of Rock Mechanics and Mining Sciences* 74:69-80, DOI: 10.1016/j.ijrmms.2014.12.002

Hasanpour R, Rostami J, Ünver B (2014) 3D finite difference model for simulation of double shield TBM tunneling in squeezing stratas. *Tunnelling and Underground Space Technology* 40(2):109-126, DOI: 10.1016/j.tust.2013.09.012

Huang N, Liu R, Jiang Y, Cheng Y, Li B (2019) Shear-flow coupling characteristics of a three-dimensional discrete fracture network-fault model considering stress-induced aperture variations. *Journal of Hydrology* 571:416-424, DOI: 10.1016/j.jhydrol.2019.01.068

Iskander M, Bathurst RJ, Omidvar M (2015) Past, present, and future of transparent soils. *Geotechnical Testing Journal* 38(5):557-573, DOI: 10.1520/GTJ20150079

Ju Y, Xie H, Zheng Z, Lu J, Mao L, Gao F, Peng RD (2014) Visualization of the complex structure and stress field inside rock by means of 3D printing technology. *Chinese Science Bulletin* 59(36):5354-5365, DOI: 10.1007/s11434-014-0579-9

Khanlari G, Rafiei B, Abdilor Y (2015) Evaluation of strength anisotropy and failure modes of laminated sandstones. *Arabian Journal of Geosciences* 8(5):3089-3102, DOI: 10.1007/s12517-014-1411-1

Lee Y, Yoo C (2006) Behavior of a bored tunnel adjacent to a line of load piles. *Tunnelling and Underground Space Technology* 21(3):370, DOI: 10.1016/j.tust.2005.12.185

Li YH, Lin ZB (2015) Innovative experimental method based on development of transparent rock mass materials for physical tests. *Chinese Journal of Geotechnical Engineering* 37(11):2030-2039, DOI: 10.11779/CJGE201511013 (in Chinese)

Li YH, Tang XJ, Yang S, Chen JW (2019) Evolution of the broken rock zone in the mixed ground tunnel based on the DSCM. *Tunnelling and Underground Space Technology* 84:248-258, DOI: 10.1016/

j.tust.2018.11.017

Li YJ, Zhang DL, Fang Q, Yu QC, Xia L (2014) A physical and numerical investigation of the failure mechanism of weak rocks surrounding tunnels. *Computers and Geotechnics* 61(3):292-307, DOI: 10.1016/j.compgeo.2014.05.017

Li YH, Zhang Q, Lin ZB, Wang XD (2016) Spatiotemporal evolution rule of rocks fracture surrounding gob-side roadway with model experiments. *International Journal of Mining Science and Technology* 26(5):895-902, DOI: 10.1016/j.ijmst.2016.05.031

Liu R, He M, Huang N, Jiang Y, Yu L (2019) A three-dimensional double-rough-walled model for simulating fluid flow through self-affine fractures during shearing by solving Navier-Stokes equations. *Journal of Rock Mechanics and Geotechnical Engineering*, DOI: 10.1016/j.jrmge.2019.07.007

Liu P, Ju Y, Ranjith PG, Zheng Z, Wang L, Wanniarachchi A (2016) Visual representation and characterization of three-dimensional hydrofracturing cracks within heterogeneous rock through 3D printing and transparent models. *International Journal of Coal Science and Technology* 3(3):284-294, DOI: 10.1007/s40789-016-0145-y

Liu R, Li B, Yu L, Jiang Y, Jing H (2018) A discrete-fracture-network fault model revealing permeability and aperture evolutions of a fault after earthquakes. *International Journal of Rock Mechanics and Mining Sciences* 107:19-24, DOI: 10.1016/j.ijrmms.2018.04.036

Mezger F, Ramoni M, Anagnostou G, Dimitrakopoulos A, Meystre N (2017) Evaluation of higher capacity segmental lining systems when tunnelling in squeezing rock. *Tunnelling and Underground Space Technology* 65:200-214, DOI: 10.1016/j.tust.2017.02.012

Ramoni M, Anagnostou G (2011) The interaction between shield, strata and tunnel support in TBM tunnelling through squeezing strata. *Rock Mechanics and Rock Engineering* 44(1):37-61, DOI: 10.1007/s00603-010-0103-8

Sun J, Liu J (2014) Visualization of tunnelling-induced strata movement in transparent sand. *Tunnelling and Underground Space Technology* 40(40):236-240, DOI: 10.1016/j.tust.2013.10.009

Teng J, Tang J, Zhang Y, Li X (2018) CT experimental study on the damage characteristics of anchored layered rocks. *KSCE Journal of Civil Engineering* 22(9):3653-3662, DOI: 10.1007/s12205-018-0425-8

Tóth Á, Gong QM, Zhao J (2013) Case studies of TBM tunneling performance in rock-soil interface mixed strata. *Tunnelling and Underground Space Technology* 38:140-150, DOI: 10.1016/j.tust.2013.06.001

Wang Y, Zhou X, Xu X (2016) Numerical simulation of propagation and coalescence of flaws in rock materials under compressive loads using the extended non-ordinary state-based Peridynamics. *Engineering Fracture Mechanics* 163:248-273, DOI: 10.1016/j.engfracmech.2016.06.013

Yang SQ, Chen M, Fang G, Wang YC, Meng B, Li YH, Jing HW (2018a) Physical experiment and numerical modelling of tunnel excavation in slanted upper-soft and lower-hard strata. *Tunnelling and Underground Space Technology* 82:248-264, DOI: 10.1016/j.tust.2018.08.049

Yang SQ, Chen M, Jing HW, Chen KF, Meng B (2017) A case study on large deformation failure mechanism of deep soft rock roadway in Xin'an coal mine, China. *Engineering Geology* 217:89-101, DOI: 10.1016/j.enggeo.2016.12.012

Yang LH, Cui YL, Zhang JZ, Zhou XP (2018b) Internal morphology of cracking of two 3-D pre-existing cross-embedded flaws under uniaxial compression. *Geotechnical Testing Journal* 41(2):329-339, DOI: 10.1520/GTJ20170189

Yang SQ, Hu B, Xu P (2019) Study on the damage-softening constitutive model of rock and experimental verification. *Acta Mechanica Sinica* 4:786-798, DOI: 10.1007/s10409-018-00833-y

Yong MT, Ming CK, Juang CH (2006) An experimental investigation of the failure mechanism of simulated transversely isotropic rocks. *International Journal of Rock Mechanics and Mining Sciences* 43(8):1163-1181, DOI: 10.1016/j.ijrmms.2006.03.011

Zhang Q, Zhang X, Wang Z, Xiang W, Xue J (2017) Failure mechanism and numerical simulation of zonal disintegration around a deep tunnel under high stress. *International Journal of Rock Mechanics and Mining Sciences* 93:344-355, DOI: 10.1016/j.ijrmms.2017.02.004

Zhang QY, Zhang XT, Xiang W, Chen XG, Cao GH, Xu XB (2013) Model test study of zonal disintegration in deep rock mass under different cavern shapes and loading conditions. *Chinese Journal of Rock Mechanics and Engineering* 32(8):1564-1571, DOI: 10.3969/j.issn.1000-6915.2013.08.007 (in Chinese)

Zhang JZ, Zhou XP (2017) Time-dependent jamming mechanism for single-shield TBM tunneling in squeezing rock. *Tunnelling and Underground Space Technology* 69:209-222, DOI: 10.1016/j.tust.2017.06.020

Zhou XP, Bi J, Qian QH (2015) Numerical simulation of crack growth and coalescence in rock-like materials containing multiple pre-existing flaws. *Rock Mechanics and Rock Engineering* 48(3):1097-1114, DOI: 10.1007/s00603-014-0627-4

Zhou XP, Cheng H, Feng YF (2014) An experimental study of crack coalescence behaviour in rock-like materials containing multiple flaws under uniaxial compression. *Rock Mechanics and Rock Engineering* 47(6):1961-1986, DOI: 10.1007/s00603-013-0511-7

Zhou XP, Fu L, Ju W, Berto F (2019) An experimental study of the mechanical and fracturing behavior in PMMA specimen containing multiple 3D embedded flaws under uniaxial compression. *Theoretical and Applied Fracture Mechanics* 101:207-216, DOI: 10.1016/j.tafmec.2019.03.002

Zhou XP, Lian YJ, Wong LNY, Berto F (2018a) Understanding the fracture behavior of brittle and ductile multi-flawed rocks by uniaxial loading by digital image correlation. *Engineering Fracture Mechanics* 199:438-460, DOI: 10.1016/j.engfracmech.2018.06.007

Zhou XP, Shou YD (2013) Excavation-induced zonal disintegration of the surrounding rock around a deep circular tunnel considering unloading effect. *International Journal of Rock Mechanics and Mining Sciences* 64(64):246-257, DOI: 10.1016/j.ijrmms.2013.08.010

Zhou XP, Yang HQ (2012) Multiscale numerical modeling of propagation and coalescence of multiple cracks in rock masses. *International Journal of Rock Mechanics and Mining Sciences* 55:15-27, DOI: 10.1016/j.ijrmms.2012.06.001

Zhou XP, Zhang YX, Ha QL (2008) Real-time computerized tomography (CT) experiments on limestone damage evolution during unloading. *Theoretical and Applied Fracture Mechanics* 50(1):49-56, DOI: 10.1016/j.tafmec.2008.04.005

Zhou XP, Zhang JZ, Wong LNY (2018b) Experimental study on the growth, coalescence and wrapping behaviors of 3D cross-embedded flaws under uniaxial compression. *Rock Mechanics Rock Engineering* 51(5):1379-1400, DOI: 10.1007/s00603-018-1406-4